THE JOURNAL OF PHYSICAL CHEMISTRY B

Article

pubs.acs.org/JPCB

Side-Chain-Dependent Helical Conformation of Amylose Alkylcarbamates: Amylose Tris(ethylcarbamate) and Amylose Tris(*n*-hexylcarbamate)

Ken Terao,*[,†] Fumihiro Maeda,[†] Keiko Oyamada,[†] Takaaki Ochiai,[†] Shinichi Kitamura,[‡] and Takahiro Sato[†]

[†]Department of Macromolecular Science, Graduate School of Science, Osaka University, 1-1 Machikaneyama-cho, Toyonaka, Osaka 560-0043, Japan

[‡]Graduate School of Life and Environmental Sciences, Osaka Prefecture University, Gakuen-cho, Nakaku, Sakai, Osaka 599-8531, Japan

Supporting Information

ABSTRACT: Eight amylose tris(ethylcarbamate) (ATEC) samples ranging in the weight-average molar mass M_w from 1.0×10^4 to 1.1×10^6 g mol^{-1} and five amylose tris(*n*-hexylcarbamate) (ATHC) samples of which M_w varies from 4.9×10^4 to 2.2×10^6 g mol^{-1} have been prepared from enzymatically synthesized amylose samples having narrow dispersity indices and no branching. Small-angle angle X-ray scattering (SAXS), light scattering, viscometry, and infrared (IR) absorption measurements were carried out for their dilute solutions, that is, ATEC in tetrahydrofuran (THF), 2-methoxyethanol (2ME), methanol (MeOH), and ATHC in THF and 1-propanol (1PrOH) to determine M_w, particle scattering functions, intrinsic viscosities, and IR spectra. SAXS and viscosity measurements were also made on ATEC in D- and L-ethyl lactates. The data were analyzed in terms of the wormlike cylinder model to estimate the helix pitch (or contour length) per residue h and the Kuhn segment length λ^{-1} (stiffness parameter, twice the persistence length). Both ATEC and ATHC have large λ^{-1} in THF, that is, 33 and 75 nm, respectively, and smaller λ^{-1} were obtained in alcohols, indicating that they have rigid helical conformation stabilized by intramolecular hydrogen bonds in THF. On the contrary, the helical structure estimated from the h value significantly depends on the alkyl side groups in a complex fashion, that is, h = 0.36 nm for ATEC, h = 0.29 nm for ATHC, and h = 0.26 nm for amylose tris(*n*-butylcarbamate) (ATBC). This is likely related to the bulkiness of side groups packed inside the amylosic helices. The solvent dependence of h, λ^{-1}, and the fraction f_{hyd} of intramolecular hydrogen bonds for ATEC can be explained by a current model as is the case with ATBC [Terao, K.; et al. *Macromolecules* **2010**, *43*, 1061], in which each contour point along the chain takes loose helical and rigid helical sequences independently.

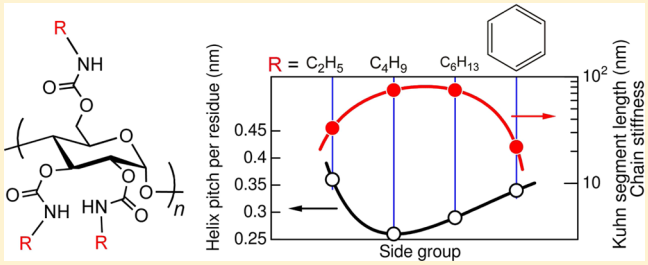

INTRODUCTION

Helix is one of the most important secondary structures of biopolymers, and thus it is significantly related to their biological functions. Thus, not only biopolymers but also a large number of synthetic helical polymers are still a hot research field.[1] To investigate physicochemical or structural properties of such polymers, its stereoregularity is definitely important. Enzymatically synthesized amylose [linear $\alpha(1\rightarrow4)$-D-glucan][2] has a strictly stereoregular primary structure and tends to form various kinds of helices[3−5] stabilized by intra- or intermolecular hydrogen-bonding (H-bonding), and furthermore the helix pitch per residue h (or contour length per repeat unit) varies from 0.1 to 0.35 nm in crystalline state. However, since amylose behaves as rather flexible polymer[6] in many solvents except for a specific solvent,[7] the local helical structure of flexible amylose chains significantly fluctuates in solution. Hence, attention has not been paid to such local structural change in solution yet. Several decades ago, it was found that amylose tris(phenylcarbamate) (ATPC) having three C═O and NH groups per repeat unit is soluble in various kinds of organic solvents, that is, some cyclic ethers, ketones, esters, and amides; ATPC has quite a stiff backbone in 1,4-dioxane[8] and significant circular dichroism, suggesting the main chain has a regular helical conformation.[9]

Recently, we found amylose tris(*n*-butylcarbamate) (ATBC, **2** in Chart 1) has 3.4 times higher chain stiffness in tetrahydrofuran (THF)[10] than ATPC in 1,4-dioxane, and this rigidity is mainly due to the intramolecular H-bonding when we analyzed their dimensional and hydrodynamic properties in terms of the wormlike chain[11] (a special case of the helical wormlike chain[12]). If the helical structure is decided only by the H-bonds as is the case with α-helices of polypeptides, it is

Received: August 11, 2012
Revised: October 4, 2012
Published: October 5, 2012

Chart 1. Chemical Structures of Amylose Tris(ethylcarbamate) (1, ATEC), Amylose Tris(*n*-butylcarbamate) (2, ATBC), and Amylose Tris(*n*-hexylcarbamate) (3, ATHC)

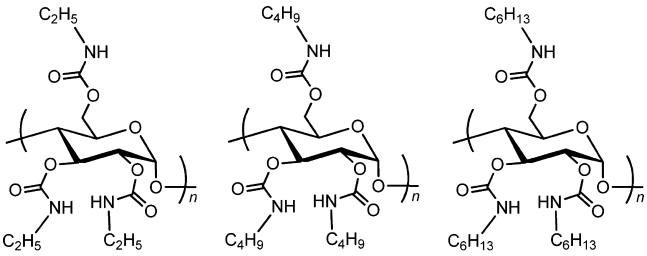

1. ATEC **2.** ATBC **3.** ATHC

hardly influenced by the slight difference in the side group. Interestingly, the *h* value estimated to be 0.26 nm is appreciably shorter than that for ATPC in 1,4-dioxane (0.34 nm);[13] these are intermediate value between double-helical A- or B-amylose (0.353 nm)[3] and single-helical V-amylose (0.10−0.13 nm).[5] These results may suggest that bulkiness of the *n*-butyl group in ATBC is related to the helical structure though the chemical natures of phenyl and *n*-butyl group are much different. To clarify the relationship between side groups and the rigid helical structure, it would be suitable to determine the *h* value in solution for amylose alkyl carbamates with different alkyl chain lengths. It should be noted that no crystal structures have been published while some calculated structures are available for amylose tris(3,5-dimethylphenylcarbamate),[14,15] which is widely used as a chiral stationary phase,[16] suggesting difficulty to determine the crystal structure.

The first aim of this paper was thus to study amylose alkylcarbamates in solution with slightly shorter and longer side groups compared with ATBC, that is, amylose tris(ethylcarbamate) (ATEC, **1** in Chart 1) and amylose tris(*n*-hexylcarbamate) (ATHC, **3**), respectively. If they have such rigid helical conformation in THF, they are compared with those for ATBC and ATPC. Solution properties in higher polar solvents were also investigated how the intra- and/or intermolecular H-bonds influence the main-chain conformation.

EXPERIMENTAL SECTION

Samples and Solvents. ATEC and ATHC samples were synthesized from an excess amount of corresponding isocyanate (ethyl- or *n*-hexyl-) and enzymatically synthesized amylose having quite narrow molar mass distribution and no branching. The reaction was performed by the same method reported previously for ATBC.[10] The reprecipitated ATEC and ATHC samples were further purified by successive fractional precipitation. Methanol (MeOH) and water were used as the solvent and the precipitant for ATEC, and THF and MeOH were used for ATHC, respectively. Appropriate middle fractions were reprecipitated to the corresponding precipitant, and they were dried in a vacuum at 80 °C for 3 days. The resultant eight ATEC (ATEC10K, ATEC32K, ATEC37K, ATEC100K, ATEC150K, ATEC400K, ATEC550K, and ATEC1100K) and six ATHC (ATHC49K, ATHC83K, ATHC300K, ATHC460K, ATHC720K, and ATHC2000K) samples were chosen for this study. The degree of substitution was estimated from the mass ratio of nitrogen to carbon to be 3.0 ± 0.2 both for ATHC and ATEC samples. The chemical structure was also confirmed by ^{1}H NMR and FT-IR spectra. The ratio of weight- to number-average molecular weight (dispersity index) determined from size exclusion chromatography equipped with a multiangle laser light scattering detector was estimated to be in the range between 1.03 and 1.2. THF, 2-methoxyethanol (2ME), MeOH, 1-propanol (1PrOH), and pyridine were fractionally distilled over CaH_2, and D-ethyl lactate (D-EL) and L-ethyl lactate (L-EL) were prepared by the method reported in ref 17.

Static Light Scattering (SLS). SLS measurements were made on a Fica-50 light scattering photometer with vertically polarized incident light of 436 nm wavelength (λ_0) (and 546 nm for three high molar mass ATHC samples in THF); see ref 13 for experimental details including optical purification. The measurements were carried out for ATEC400K, ATEC550K, and ATEC1100K in 2ME and THF at 25 °C and ATHC83K, ATHC300K, ATHC460K, ATHC720K, and ATHC2000K in 1PrOH and THF at 25 °C to determine the weight-average molar mass M_w, the second virial coefficient, the particle scattering function $P(q)$, and the *z*-average radius of gyration $\langle S^2\rangle_z$. See Supporting Information for the plots of $P(q)^{-1/2}$ vs q^2, where q denotes the magnitude of the scattering vector. The obtained M_w's in different solvents are consistent within the experimental error and are summarized in the Supporting Information with $\langle S^2\rangle_z$. The second virial coefficients are in the range between 8×10^{-5} and 1×10^{-3} mol cm^3 g^{-2}; thus, they are good solvent systems. The specific refractive indices $\partial n/\partial c$ at 25 °C were determined to be 0.0849 cm^3 g^{-1} for ATEC in THF, 0.0919 cm^3 g^{-1} for ATEC in 2ME, 0.0876 cm^3 g^{-1} for ATHC in THF, 0.0989 cm^3 g^{-1} for ATHC in 1PrOH all at λ_0 = 436 nm and 0.0867 cm^3 g^{-1} for ATHC in THF at λ_0 = 546 nm.

Ultracentrifugation. Sedimentation equilibrium measurements were carried out for ATEC10K, ATEC32K, ATEC37K, ATEC100K, and ATEC150K in 2ME and for ATHC49K in THF all at 25 °C using a Beckman Optima XL-1 analytical ultracentrifuge at the rotor speed from 8000 to 20 000 rpm to determine M_w and *z*-average molar mass M_z (see refs 13 and 18 for experimental details and data analysis). The $\partial n/\partial c$ values at the used wavelength (675 nm) were estimated to be 0.088 and 0.086 cm^3 g^{-1} for ATEC in 2ME and ATHC in THF, respectively. The partial specific volume for the two systems was evaluated to be 0.754 and 0.884 cm^3 g^{-1}, respectively, by using an Anton Paar DMA5000 density meter.

Small-Angle X-ray Scattering (SAXS). SAXS measurements were made for ATEC10K and ATEC32K (or ATEC37K) in MeOH, 2ME, THF, D-EL, and L-EL and for ATHC49K in THF and 1PrOH all at 25 °C at the BL40B2 beamline in SPring-8 and the BL-10C beamline in KEK-PF (see ref 13 for the experimental details). The wavelength, camera length, and accumulation time were chosen to be 0.10−0.15 nm, 1500−2000 mm, and 300 s, respectively. The Berry square root plots[19] were utilized to determine both $P(q)$ and $\langle S^2\rangle_z$ from the excess scattering intensities for four solutions with different polymer mass concentration c since this plot has wider linear region for both flexible and rigid linear chains than those for the Zimm and Guinier plots.[8a,20]

Viscometry. Relative viscosities for ATEC samples in THF, D-EL, L-EL, 2ME, and MeOH and for ATHC samples in THF and 1PrOH all at 25 °C were determined for four solutions with different c by using Ubbelohde-type viscometers to determine the intrinsic viscosity $[\eta]$ and the Huggins constant k'. The latter values (k') were obtained to be from 0.3 to 1.0 for ATEC and from 0.3 to 0.7 for ATHC.

Infrared Absorption. FT-IR measurements were made for ATEC400 K in THF, 2ME, and MeOH and for ATHC720 K in THF and 1PrOH all at 25 °C on a Bio-Rad FTS-300 or a Jasco FT/IR 4200 Fourier transform infrared spectrometer with a solution cell made of CaF_2 (0.05 mm path length).

RESULTS

Dimensional and Hydrodynamic Properties. Square roots of $\langle S^2 \rangle_z$ plotted logarithmically against M_w in Figure 1

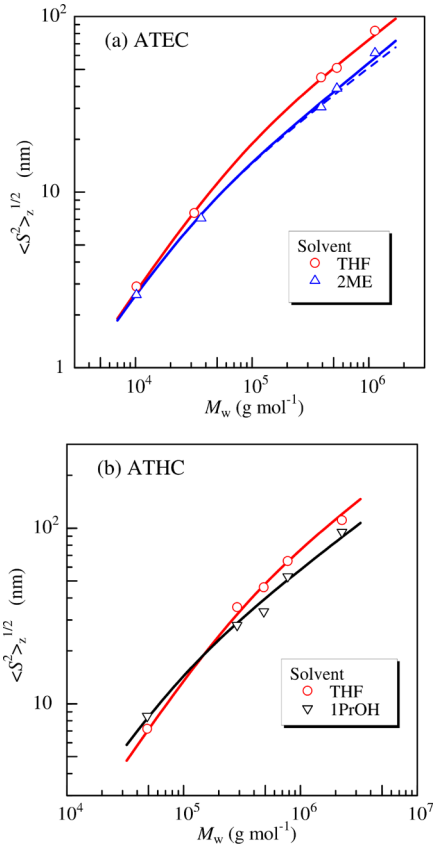

Figure 1. Molar mass dependence of z-average radii of gyration $\langle S^2 \rangle_z^{1/2}$ for ATEC (a) and ATHC (b) in THF (circles), 2ME (triangles), and 1PrOH (inversed triangles) all at 25 °C. Solid curves: theoretical values for the wormlike chain model with the parameters in Table 1; a dashed curve: the theoretical values for $B = 0$.

have large slopes from 0.7 to 0.9 in lower M_w range, and they become smaller with increasing M_w. Similar behavior is also found for molar mass dependence of $[\eta]$ displayed in Figure 2. These are typical for the wormlike chain. Furthermore, the Holtzer plots[21] (Figure 3) for ATEC32K in THF have a plateau at a q range between 0.2 and 0.8 nm^{-1} whereas that for ATEC37K in MeOH has a peak at 0.3 nm^{-1}, indicating that the chain stiffness of ATEC is much higher in THF than that in MeOH.

Solution IR Spectra. IR spectra for amide I band mainly reflect C═O stretching,[10,15] and their absorption wavenumber is significantly influenced by the environment around the C═O group, such as H-bonding. Indeed, we recently analyzed the IR spectra for ATBC in nine solvents and their mixtures to estimate the number fraction of intramolecular H-bonding C═O groups f_{hyd}.[10] Figure 4 displays IR spectra for ATEC in THF, 2ME, and MeOH and for ATHC in THF and 1PrOH. Both the two polymers in THF have two peaks while ATEC in MeOH

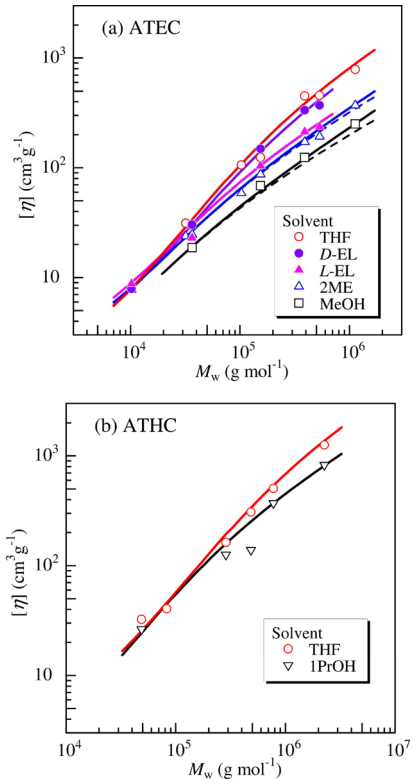

Figure 2. Molar mass dependence of intrinsic viscosities $[\eta]$ for ATEC (a) and ATHC (b) in THF (unfilled circles), D-EL (filled circles), L-EL (filled triangles), 2ME (unfilled triangles), MeOH (squares), and 1PrOH (inversed triangles) all at 25 °C. Solid curves: theoretical values for the wormlike cylinder model with the parameters in Table 1; dashed curves: theoretical values for $B = 0$.

has a broad single peak in between the peaks in THF, indicating that about 50% of C═O groups form intramolecular H-bonds in THF. But in MeOH, intermolecular H-bonds between C═O and OH group of the solvent are predominant. Thus, C═O groups in other solvents may consist of intramolecular H-bonding (1698 and 1700 cm^{-1}), free (1725−1740 cm^{-1}), and intermolecular H-bonding C═O groups (1720 cm^{-1}) with solvent molecules, as is the case with ATBC, and hence the peaks were separated into three. The fractions f_{hyd} values at 1698 or 1700 cm^{-1} are listed along with the wormlike chain parameters estimated later (Table 2).

DISCUSSION

Wormlike Chain Analysis. According to the theoretical formulation of $P(q)$ for the wormlike cylinder,[22] $P(q)$ is calculated with the parameters, that is, the contour length L, the Kuhn segment length λ^{-1} (stiffness parameter), and the chain diameter d; L is proportional to the molar mass M of the polymer thus related to the molar mass per unit contour length M_L by $L = M/M_L$. The two parameters M_L and d were unequivocally determined from the curve fitting in the higher q range since the resultant theoretical solid curves calculated with the parameters in Table 1 are equivalent to the dashed curves for the straight cylinder in the q range. The other parameter (λ^{-1}) was determined to fit the peak in low q region. The variation for the parameters determined from the different M_w samples are in the error range shown in Table 1. However, λ^{-1} for ATEC in THF and D-EL and for ATHC in THF and 1PrOH cannot be determined because of the small deviation of

dx.doi.org/10.1021/jp307998t | J. Phys. Chem. B 2012, 116, 12714−12720

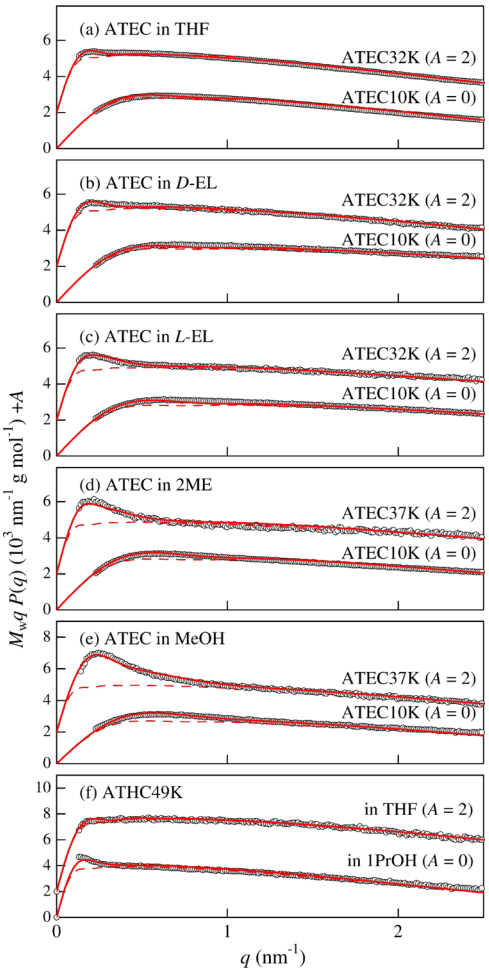

Figure 3. Reduced Holtzer plots for ATEC in THF (a), in D-EL (b), in L-EL (c), in 2ME (d), in MeOH (e), and ATHC in THF and 1PrOH (f) all at 25 °C. Solid curves: theoretical values for the wormlike cylinder model with the parameters in Table 1; dashed curves: theoretical values for the rod limit ($\lambda^{-1} = \infty$). For clarity, the ordinate values of $M_w qP(q)$ are shifted by an arbitrary constant (A) indicated in parentheses.

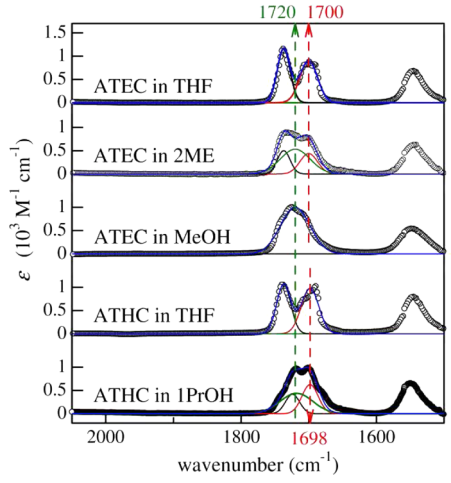

Figure 4. IR spectra (molar absorption coefficient ε vs wavenumber) for ATEC and ATHC in indicated solvents at 25 °C.

the data points from the straight cylinder. This is reasonable because the theoretical solid curves for the wormlike cylinder

Table 1. Wormlike Chain Parameters for ATEC in Tetrahydrofuran (THF), D-Ethyl Lactate (D-EL), L-Ethyl Lactate (L-EL), 2-Methoxyethanol (2ME), and Methanol (MeOH) and for ATHC in THF and 1-Propanol (1PrOH) All at 25 °C

method	M_L (g mol^{-1} nm^{-1})	λ^{-1} (nm)	d (nm)	B (nm)
ATEC in THF				
$P(q)$	1060 ± 30	33[a]	1.3 ± 0.1	
$\langle S^2\rangle_z$	1020 ± 50	35 ± 3		
$[\eta]$	1040[a]	32 ± 3	1.6 ± 0.2	
ATEC in D-EL				
$P(q)$	1080 ± 30	27[a]	1.1 ± 0.2	
$[\eta]$	1080[a]	27 ± 2	1.8 ± 0.2	
ATEC in L-EL				
$P(q)$	990 ± 30	16 ± 3	1.0 ± 0.1	
$[\eta]$	990[a]	15 ± 1	1.9 ± 0.2	
ATEC in 2ME				
$P(q)$	990 ± 30	13 ± 3	1.1 ± 0.1	
$\langle S^2\rangle_z$	1000 ± 50	16 ± 2		1 ± 1
$[\eta]$	1000[a]	13 ± 1	1.8 ± 0.2	0.5 ± 0.5
ATEC in MeOH				
$P(q)$	990 ± 30	8.5 ± 1.0	1.1 ± 0.1	
$[\eta]$	990[a]	9 ± 1	1.4 ± 0.2	1 ± 1
ATHC in THF				
$P(q)$	1900 ± 40	75[a]	1.0 ± 0.2	
$\langle S^2\rangle_z$	1900 ± 100	70 ± 5		
$[\eta]$	1900[a]	80 ± 5	3.5 ± 1.0	
ATHC in 1PrOH				
$P(q)$	1330 ± 40	30[a]	1.4 ± 0.2	
$\langle S^2\rangle_z$	1400 ± 100	30 ± 5		
$[\eta]$	1400[a]	30 ± 5	1.6 ± 1.0	

[a]Assumed values.

with λ^{-1} obtained from $\langle S^2\rangle_z$ and/or $[\eta]$ well reproduce the experimental data. It should be noted that the radius of gyration calculated by eq 1 fairly reproduces the experimental $\langle S^2\rangle_z$ for the samples shown in Figure 3.

When the Benoit–Doty equation[23] for the radius of gyration $\langle S^2\rangle_0$ of the unperturbed wormlike chain

$$\langle S^2\rangle_0 = \frac{L}{6\lambda} - \frac{1}{4\lambda^2} + \frac{1}{4\lambda^3 L} - \frac{1}{8\lambda^4 L^2}[1 - \exp(-2\lambda L)] \quad (1)$$

is combined with the Domb–Barrett equation[24] for the expansion factor in the quasi-two-parameter (QTP) theory,[12,25] the radius of gyration for given molar mass is determined by the three parameters: M_L, λ^{-1}, and the excluded volume strength B. The equations used are summarized in a book chapter.[26] The former two parameters, M_L and λ^{-1}, were determined by the curve fitting procedure for ATEC in THF and 2ME and for ATHC in THF and 1PrOH and are listed in Table 1. The last parameter B was not determined for the three systems other than ATEC in 2ME since the expansion factor was essentially the same as unity for the possible B values; indeed, the deviation between solid and dashed curves even for ATEC in 2ME is at most 7% for the highest molar mass ATEC sample. It should be noted the chain thickness effects on $\langle S^2\rangle$ estimated from $d^2/8$ for the wormlike cylinder[27] is negligibly small (<3%) in the M_w range investigated.

dx.doi.org/10.1021/jp307998t | J. Phys. Chem. B 2012, 116, 12714–12720

Intrinsic viscosities for the perturbed wormlike chain for given M are calculated from the four parameters M_L, λ^{-1}, d, and B when we utilize the Yamakawa–Fujii–Yoshizaki theory[12,28] for unperturbed wormlike chain and the Barrett function[29] with the QTP theory. See also ref 26 for the equations. Since all the four parameters are hard to determine only from our $[\eta]$ data, the curve fitting procedure was employed assuming M_L determined from $P(q)$ and/or $\langle S^2\rangle_z$. While the two parameters λ^{-1} and d are unequivocally estimated, the viscosity expansion factor is substantially the same as unity for ATEC in THF, D-EL, and L-EL and for ATHC in the two solvents; thus, the parameter B was not determined for the five systems. The theoretical values calculated with the resultant parameters summarized in Table 1 closely fit the experimental data in Figure 2. The obtained λ^{-1} values are consistent with those determined from $P(q)$ and/or $\langle S^2\rangle_z$, indicating that the wormlike chain is a good model for ATEC and ATHC chains. It should be noted that d determined from $[\eta]$ is appreciably larger than that from $P(q)$ since the latter reflects the electron density profile of the chain cross section and the former is the hydrodynamic diameter. Similar behavior has been also found for ATBC.[10]

Wormlike Chain Parameters and Rigid helical Structures in THF. The mean values of λ^{-1} and the helix pitch per residue h calculated as $h = M_0/M_L$ are summarized in Table 2 along with f_{hyd} where M_0 is molar mass of the repeat unit of the polymer (375.4 g mol^{-1} for ATEC and 543.7 g mol^{-1} for ATHC). This table includes our previous data for ATBC.[10,17,30] While f_{hyd} increases with decreasing the polarity of the solvent and reaches about 0.5 in THF as is the case with ATBC, λ^{-1} for ATEC and ATHC tends to increase and that for ATHC in THF is equivalent to the highest value for single-chain polysaccharide derivatives, that is, ATBC in THF (λ^{-1} = 75 nm),[10] amylose tris(3,5-dimethylphenylcarbamate) in 4-methyl-2-pentanone (λ^{-1} = 73 nm),[31] and Curdlan tris-(phenylcarbamate) in THF (λ^{-1} = 57 nm).[32] On the other hand, the h value for ATEC in THF is about 40% larger than that for ATBC in the same solvent and ATHC has an intermediate value. Assuming 6-fold left-handed helices, the helical structures of the main chain for the three h's (0.36, 0.29, and 0.26 nm) are illustrated in Figure 5a. The internal rotation angle (ϕ, ψ), shown in panel b, for the three helices are (91°, −147°), (81°, −130°), and (80°, −125°), respectively, where ϕ = O(5)–C(1)–O(4)–C(4) and ψ = C(1)–O(4)–C(4)–C(5). In the conformational energy map for maltose unit proposed by Shimada et al.,[33] those internal rotational angles are in a relatively low energy region, so that those helix states of amylose without the side chain are energetically favorable. On the other hand, the side-chain bulkiness also affects the main-chain helical structure of amylose carbamates. It is seen that the space inside the helices becomes narrower with increasing h value. Thus, the smaller ethyl group on the ATEC side chain may permit a larger h value (≈0.36 nm), but the larger butyl group on the ATBC side chain may not. Indeed, the side group of the sixth position of ATBC may locate inside the helices having a smaller h = 0.25 nm from the molecular dynamics simulation shown in our previous paper.[10] On the contrary, it is reasonably supposed that such short h value is no more stable for amylose carbamates having bulkier side groups since too large side groups may not be inside the helix, and hence the resultant helical structure may become thinner with larger h value. Indeed, the h value of ATHC in THF is slightly larger than that for ATBC in the same solvent, and furthermore, ATPC of which the phenyl group should be bulkier than n-hexyl group has a larger h value of 0.34 nm in 1,4-dioxane[13] (Figure 5b). Furthermore, the chain stiffness tends to become higher with decreasing h in THF (or in 1,4-dioxane). These clearly indicate that the bulkiness of side groups of amylose carbamates is definitely important for both the local helical structure and the chain stiffness. This is a unique feature of amylose carbamates while α-helical structure of polypeptides is almost independent of amino acids.

Another interesting finding is that λ^{-1} for ATEC in ethyl lactates significantly depends on the chirality of the solvent, that

Table 2. Values of the Helix Pitch per Residue h, the Kuhn Segment Length λ^{-1}, and the Number Fraction f_{hyd} of Intramolecular H-Bonding C═O Groups for ATEC, ATHC, and ATBC

polymer	solvent	T (°C)	h (nm)	λ^{-1} (nm)	f_{hyd}
ATEC	THF	25	0.36 ± 0.02	33 ± 3	0.46
ATEC	D-EL	25	0.35 ± 0.02	27 ± 2	
ATEC	L-EL	25	0.38 ± 0.02	15 ± 2	
ATEC	2ME	25	0.38 ± 0.02	14 ± 2	0.26
ATEC	MeOH	25	0.38 ± 0.02	9 ± 1	0
ATHC	THF	25	0.29 ± 0.02	75 ± 5	0.53
ATHC	1PrOH	25	0.39 ± 0.02	30 ± 3	0.34
ATBC[a]	THF	25	0.26 ± 0.01	75 ± 5	0.52
ATBC[c]	D-EL	25	0.26 ± 0.01	49 ± 4	
ATBC[b]	2BuOH[d]	45	0.25 ± 0.01	40 ± 5	0.41
ATBC[b]	2EE[e]	25	0.25 ± 0.01	38 ± 4	0.39
ATBC[c]	DL-EL[f]	25	0.26 ± 0.01	38 ± 3	
ATBC[c]	L-EL	25	0.26 ± 0.01	32 ± 2	
ATBC[b]	1PrOH	40	0.28 ± 0.01	25 ± 2	0.33
ATBC[b]	2PrOH[g]	35	0.29 ± 0.01	20 ± 2	0.29
ATBC[a]	MeOH	25	0.32 ± 0.01	11 ± 2	0

[a]Reference 10. [b]Reference 30. [c]Reference 17. [d]2-Butanol. [e]2-Ethoxyethanol. [f]DL-Ethyl lactate. [g]2-Propanol.

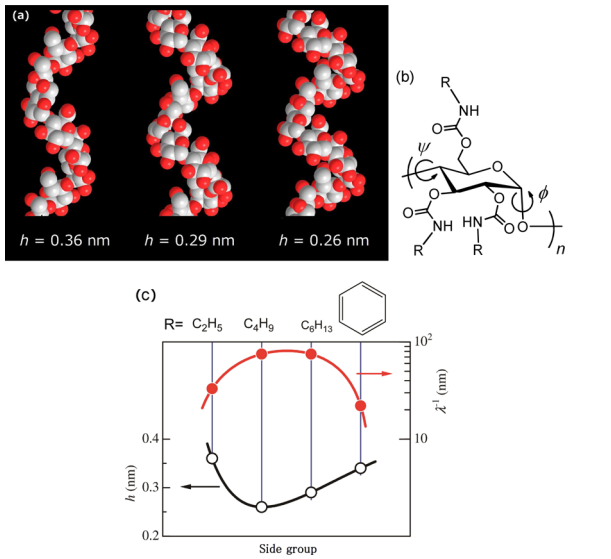

Figure 5. (a) Schematic representation of the amylosic main chain for h = 0.36, 0.29, and 0.26 nm. (b) Internal rotation angles ϕ and ψ for amylose carbamates. (c) h and λ^{-1} values for ATEC, ATBC,[10] ATHC, and ATPC[13] in THF or 1,4-dioxane.

dx.doi.org/10.1021/jp307998t | J. Phys. Chem. B 2012, 116, 12714–12720

is, in D-EL and in L-EL. The ratio (1.8) of λ^{-1} in the two solvents is larger than that for ATBC in the same solvents (1.53).[17] Considering the higher chain stiffness of ATBC in D-EL is due to more intramolecular H-bonds,[17] ATEC in D-EL should have larger numbers of intramolecular H-bonds than that in L-EL.

Solvent Dependence of the Chain Conformation. We recently showed that the relationship among h, λ^{-1}, and f_{hyd} for ATBC in 12 solvents is well explained by a two-state wormlike chain (TSWC) model,[10,30,17] in which each chain consists of random sequences of semiflexible (loose helical, L) and rigid helical (R) units. Its radius of gyration is characterized by the Kuhn segment lengths ${\lambda_L}^{-1}$ and ${\lambda_R}^{-1}$ for pure L and R chains and the helix pitches per residue h_L and h_R, respectively. In this model, both h and λ^{-1} of the entire chain can be written as

$$h = fh_R + (1 - f)h_L \tag{2}$$

$$\lambda h = f\lambda_R h_R + (1 - f)\lambda_L h_L \tag{3}$$

Here, f is the fraction of the rigid helical unit, which may be related to the number fraction f_{hyd} of intramolecular H-bonding C═O groups by

$$f = \frac{f_{hyd} - f_{hyd,L}}{f_{hyd,R} - f_{hyd,L}} \tag{4}$$

with $f_{hyd,R}$ and $f_{hyd,L}$ being f_{hyd} at f = 1 and 0, respectively. For ATBC, $f_{hyd,R}$ and $f_{hyd,L}$ were estimated to be 0.55 ± 0.03 and 0, respectively.[10,30] Alternatively, if we eliminate f from these equations, h can be written as

$${h^{-1}} - {h_L}^{-1} = -\frac{{h_R}^{-1} - {h_L}^{-1}}{\lambda_L - \lambda_R}(\lambda - \lambda_L) \tag{5}$$

Figure 6 shows the plots of h and λh for ATEC, ATBC, and ATHC against f_{hyd}, along with the plots of h^{-1} vs λ. The plots of h^{-1} vs λ for both ATEC and ATBC are linear, being consistent with eq 5. This indicates that the TSWC model well explains the solvent dependence of wormlike chain parameters. However, the values of h of ATEC and ATBC are not identical both at f_{hyd} = 0 and 0.55, which implies that the rigid and loose helical conformations are determined by not only f_{hyd} but also the steric hindrance due to the side chain.

On the other hand, the plot of h vs f_{hyd} for ATHC has much larger negative slope than that for ATBC and ATEC. The h value obtained for amylose carbamates, that is, ATBC, ATPC, amylose tris(3,5-dimethylphenylcarbamate), and amylose-2-acetyl-3,6-bis(phenylcarbamate), are in between 0.25 and 0.42 nm.[13,31,34,35] Therefore, if we apply the TSWC model to ATHC, $f_{hyd,L}$ must be considerably larger than 0, and ${\lambda_L}^{-1}$ must be much larger than those for ATBC and ATEC. The bulky n-hexyl group on ATHC may restrict the freedom of the internal rotation in the loose helical state, which can prevent the internal rotational fluctuation from increasing with further decreasing the degree intramolecular H-bonding from $f_{hyd,L}$. Similar behavior was recently reported for ATPC that both the h and λ^{-1} values increase with increasing molar volume of the solvent having a C═O group (ketones and esters).[34]

CONCLUSIONS

Both ATEC and ATHC have rigid helical structure stabilized by intramolecular H-bonds in THF and the chain stiffness significantly decreases with decreasing the H-bonds in alcohols as is the case with ATBC, indicating that the helices of amylose alkyl carbamates are stiffened by the intramolecular H-bond. However, while the α-helical structure of polypeptides is irrespective of their side chain, the helix pitch per residue of the helices of amylose alkyl carbamates in THF and alcohols depends significantly on the alkyl chain length in a complex fashion. This indicates that the helical structure of amylose alkyl carbamates is influenced not only by the main-chain internal rotation potential and intramolecular H-bonds but also by the side-chain bulkiness.

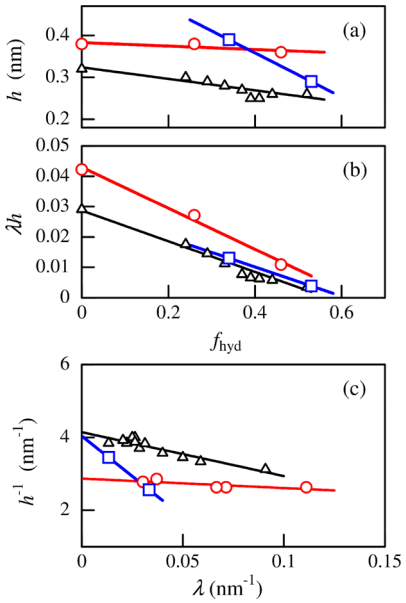

Figure 6. Plots of h vs f_{hyd} (a), λh vs f_{hyd} (b), and h^{-1} vs λ (c) for ATEC (circles), ATHC (squares), and ATBC[10,17,30] (triangles).

ASSOCIATED CONTENT

Supporting Information

Raw light scattering data (Berry plots) and numerical results of M_w, $\langle S^2\rangle_z$, and $[\eta]$. This material is available free of charge via the Internet at http://pubs.acs.org.

AUTHOR INFORMATION

Corresponding Author

*E-mail: kterao@chem.sci.osaka-u.ac.jp.

Notes

The authors declare no competing financial interest.

ACKNOWLEDGMENTS

The synchrotron radiation experiments were performed at the BL40B2 in SPring-8 with the approval of the Japan Synchrotron Radiation Research Institute (JASRI) (Proposal Nos. 2007A1034, 2007B1296, 2008A1313, 2009A1049, and 2010A1587) and at the BL-10C in KEK-PF under the approval of the Photon Factory Program Advisory Committee (No. 2010G080). The authors thank Prof. Yoji Inoko (Osaka Univ.) for SAXS measurements in KEK-PF. This work was partially supported by Grant-in-Aid for Young Scientists (#23750128) from Japan Society for the Promotion of Science (JSPS).

REFERENCES

(1) (a) Hill, D. J.; Mio, M. J.; Prince, R. B.; Hughes, T. S.; Moore, J. S. *Chem. Rev.* **2001**, *101*, 3893−4011. (b) Gellman, S. H. *Acc. Chem.*

Res. **1998**, *31*, 173−180. (c) Yashima, E.; Maeda, K.; Iida, H.; Furusho, Y.; Nagai, K. *Chem. Rev.* **2009**, *109*, 6102−6211.
(2) (a) Kadokawa, J.-I. *Chem. Rev.* **2011**, *111*, 4308−4345. (b) Kitamura, S.; Yunokawa, H.; Mitsuie, S.; Kuge, T. *Polym. J.* **1982**, *14*, 93−99. (c) Waldmann, H.; Gygax, D.; Bednarski, M. D.; Shangraw, W. R.; Whitesides, G. M. *Carbohydr. Res.* **1986**, *157*, c4−c7. (d) Kitamura, S. In *The Polymeric Materials Encyclopedia, Synthesis Properties and Applications*; Salamone, C., Ed.; CRC Press: New York, 1996; Vol. *10*, pp 7915−7922.
(3) (a) Popov, D.; Buléon, A.; Burghammer, H.; Chanzy, N.; Montesanti, N.; Putaux, J.-L.; Potocki-Veronese, G.; Riekel, C. *Macromolecules* **2009**, *42*, 1167−1174. (b) Takahashi, Y.; Kumano, T.; Nishikawa, S. *Macromolecules* **2004**, *37*, 6827−6832.
(4) Putseys, J. A.; Lambert, L.; Delcour, J. A. *J. Cereal Sci.* **2010**, *51*, 238−247.
(5) (a) Nishiyama, Y.; Mazeau, K.; Morin, M.; Cardoso, M. B.; Chanzy, H.; Putaux, J.-L. *Macromolecules* **2010**, *43*, 8628−8636. (b) Cardoso, M. B.; Putaux, J.-L.; Nishiyama, Y.; Helbert, W.; Hytch, M.; Silveira, N. P.; Chanzy, H. *Biomacromolecules* **2007**, *8*, 1319−1326.
(6) (a) Nakanishi, Y.; Norisuye, T.; Teramoto, A.; Kitamura, S. *Macromolecules* **1993**, *26*, 4220−4225. (b) Norisuye, T. *Polym. J.* **1994**, *26*, 1303−1307.
(7) Seger, B.; Aberle, T.; Burchard, W. *Carbohydr. Polym.* **1996**, *31*, 105−112.
(8) (a) Burchard, W. In *Soft-Matter Characterization*; Borsali, R., Pecora, R., Eds.; Springer: Berlin, Germany, 2008; pp 465−603. (b) Burchard, W. *Makromol. Chem.* **1965**, *88*, 11−28.
(9) Bittiger, H.; Keilich, G. *Biopolymers* **1969**, *7*, 539−556.
(10) Terao, K.; Murashima, M.; Sano, Y.; Arakawa, S.; Kitamura, S.; Norisuye, T. *Macromolecules* **2010**, *43*, 1061−1068.
(11) Kratky, O.; Porod, G. *Recl. Trav. Chim. Pays-Bas* **1949**, *68*, 1106−1122.
(12) (a) Yamakawa, H. *Helical Wormlike Chains in Polymer Solutions*; Springer: Berlin, 1997. (b) Yamakawa, H. *Polym. J.* **1999**, *31*, 109−119.
(13) Terao, K.; Fujii, T.; Tsuda, M.; Kitamura, S.; Norisuye, T. *Polym. J.* **2009**, *41*, 201−207.
(14) Yamamoto, C.; Yashima, E.; Okamoto, Y. *J. Am. Chem. Soc.* **2002**, *124*, 12583−12589.
(15) Kasat, R. B.; Zvinevich, Y.; Hillhouse, H. W.; Thomson, K. T.; Wang, N.-H. L.; Franses, E. I. *J. Phys. Chem. B* **2006**, *110*, 14114−14122.
(16) Ikai, T.; Okamoto, Y. *Chem. Rev.* **2009**, *109*, 6077−6101.
(17) Arakawa, S.; Terao, K.; Kitamura, S.; Sato, T. *Polym. Chem.* **2012**, 472−478.
(18) Norisuye, T.; Yanaki, T.; Fujita, H. *J. Polym. Sci., Polym. Phys. Ed.* **1980**, *18*, 547−558.
(19) Berry, G. C. *J. Chem. Phys.* **1966**, *44*, 4550−4564.
(20) Terao, K.; Mays, J. W. *Eur. Polym. J.* **2004**, *40*, 1623−1627.
(21) Holtzer, A. *J. Polym. Sci.* **1955**, *17*, 432−434.
(22) Nakamura, Y.; Norisuye, T. *J. Polym. Sci., Part B: Polym. Phys.* **2004**, *42*, 1398−1407.
(23) Benoit, H.; Doty, P. *J. Phys. Chem.* **1953**, *57*, 958−963.
(24) Domb, C.; Barrett, A. J. *Polymer* **1976**, *17*, 179−184.
(25) (a) Yamakawa, H.; Stockmayer, W. H. *J. Chem. Phys.* **1972**, *57*, 2843−2854. (b) Shimada, J.; Yamakawa, H. *J. Chem. Phys.* **1986**, *85*, 591−599.
(26) Nakamura, Y.; Norisuye, T. In *Soft-Matter Characterization*; Borsali, R., Pecora, R., Eds.; Springer: Berlin, 2008; Vol. *1*, pp 236−286.
(27) Konishi, T.; Yoshizaki, T.; Saito, T.; Einaga, Y.; Yamakawa, H. *Macromolecules* **1990**, *23*, 290−297.
(28) (a) Yamakawa, H.; Fujii, M. *Macromolecules* **1974**, *7*, 128−135. (b) Yamakawa, H.; Yoshizaki, T. *Macromolecules* **1980**, *13*, 633−643.
(29) Barrett, A. J. *Macromolecules* **1984**, *17*, 1566−1572.
(30) Sano, Y.; Terao, K.; Arakawa, S.; Ohtoh, M.; Kitamura, S.; Norisuye, T. *Polymer* **2010**, *51*, 4243−4248.
(31) Tsuda, M.; Terao, K.; Nakamura, Y.; Kita, Y.; Kitamura, S.; Sato, T. *Macromolecules* **2010**, *43*, 5779−5784.
(32) Ochiai, M.; Terao, K.; Nakamura, Y.; Yoshikawa, C.; Sato, T. *Polymer* **2012**, *53*, 3946−3950.
(33) Shimada, J.; Kaneko, H.; Takada, T.; Kitamura, S.; Kajiwara, K. *J. Phys. Chem. B* **2000**, *104*, 2136−2147.
(34) Fujii, T.; Terao, K.; Tsuda, M.; Kitamura, S.; Norisuye, T. *Biopolymers* **2009**, *91*, 729−736.
(35) Tsuda, M.; Terao, K.; Kitamura, S.; Sato, T. *Biopolymers* **2012**, *97*, 1010−1017.